Auralization of an unmanned aerial vehicle under propeller phase control

Kyle A. Pascioni[a)]
National Institute of Aerospace
Hampton, VA 23666

Stephen A. Rizzi[b)]
Aeroacoustics Branch
NASA Langley Research Center
Hampton, VA 23681

Aric R. Aumann[c)]
Science Applications International Corporation
Hampton, VA 23666

ABSTRACT

Community noise has been identified as a major barrier to entry into service of unmanned aerial vehicle platforms. Common among such vehicle architectures is a distributed electric propulsion system, in which many propellers and/or rotors are used for thrust and/or lift. A promising noise reduction technique was recently developed to favorably modify the vehicle source noise directivity, by adjusting the relative azimuthal position of the prop/rotor blades between propulsors. Under idealized conditions, such phase control can yield noise reductions on the order of 20 dB at a ground observer relative to the average case having a random phase distribution. However, human perception of the resulting noise may not be fully captured by such a simple acoustic measure. To this end, this paper undertakes the auralization of the tonal vehicle noise. Specifically, total propeller tonal noise is optimized over a set of observer zones, e.g., 45 deg. wedges, around the vehicle. Each zone represents a unique set of relative phases. The forward flight of the vehicle adjacent to a noise-sensitive area is simulated by prescribing a series of zones over the flight path having minimum noise in the direction of the observer. Auralizations and their associated metrics are compared with a reference condition.

1. INTRODUCTION

Emerging aviation sectors such as Urban Air Mobility (UAM) are expected to increase community noise, potentially to a point where their operations may one day be restricted. To minimize annoyance and to increase the likelihood of success for the UAM market, novel design and operational procedures with acoustics in mind are essential. Human perception must also be accounted for in order to obtain a measure of effectiveness of a given design or

[a)] kyle.a.pascioni@nasa.gov
[b)] s.a.rizzi@nasa.gov
[c)] aric.a.aumann@nasa.gov

operating state, in addition to what might be predicted by noise certification metrics. Since few, if any, UAM vehicles are currently in service, auralization of the sound using source noise predictions provides a means of assessing human response to community noise.

In terms of modifying vehicle characteristics for low-noise operation, a method similar to synchrophasing the propellers of traditional aircraft[1–3] is employed herein. Phase control involves directivity modification of the multipropeller/multirotor system noise via relative azimuthal positioning of propellers rotating at equivalent rates. In contrast to the studies just mentioned, the objective function is tailored to reducing community noise rather than cabin noise.

The Greased Lightning 10 (GL-10)[4] is the chosen vehicle platform to demonstrate the approach. Equipped with vertical take-off and landing (VTOL) capabilities and distributed electric propulsion (DEP), this configuration closely resembles many UAM vehicle concepts. Under ideal conditions, phase control can greatly reduce the average sound pressure level across a 45° wedge of observers in forward flight.[5] Realistically, this reduction may degrade for a number of reasons, such as coherence loss due to spatial separation of the propellers, propulsion-airframe interactions, turbulence ingestion, atmospheric turbulence, etc. With that in mind, this work seeks to lay the foundation of auralizing a UAM-like vehicle under phase control rather than claiming accuracy in the source predictions. Specifically, the methods to analyze this problem are discussed and showcased through flyover simulations. Ongoing work is tailored toward understanding the validity of the embedded assumptions in the source noise prediction, at which time potential benefits of phase control may be better estimated.

This paper begins by introducing the GL-10 aircraft and the flight path geometry for the simulation. Source noise modeling and propagation are discussed along with the details of phase control. Then, various noise metrics from flyover events are assessed through auralization.

2. VEHICLE AND OPERATING CONDITIONS

The GL-10 is a 50% scale unmanned aerial vehicle, chosen for its commonalities with many UAM vehicle concepts. Outfitted with ten propulsors (each with three blades having a radius $R = 0.2032$ m), tonal propeller noise is expected to be a dominant noise source during forward flight. Figure 1(a) is a rendering of the GL-10 showing the eight wing-mounted and two tail-mounted propulsors. Note the counter-rotating directions for adjacent propellers along the wing.

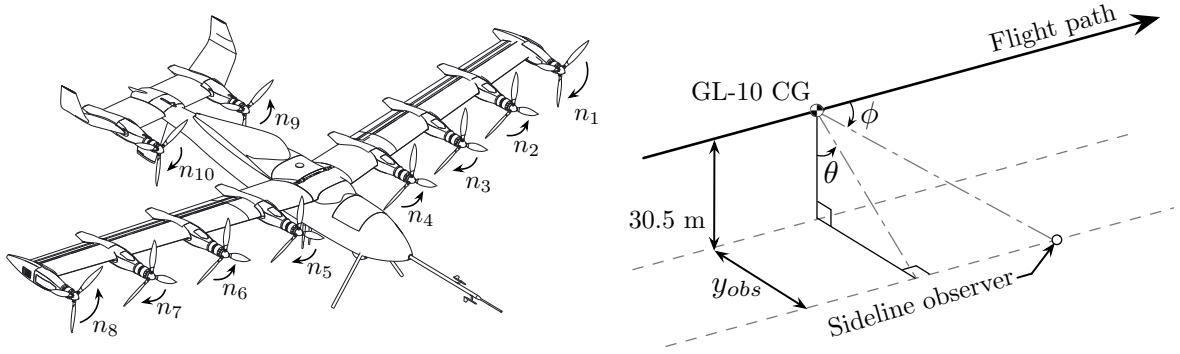

(a) (b)

Fig. 1 – The (a) GL-10 rendering denoting rotation direction of each propeller, labeled n_1-n_{10}, and (b) the specified flight path and stationary observer location.

Flyover events are simulated to understand the aerodynamic noise to which ground observers may be subjected.. For simplicity, the GL-10 will fly straight and level at an altitude of 30.5 m. In this work, ϕ and θ are defined as the polar and azimuthal emission angle, respec-

tively. As shown in Fig. 1(b), a stationary observer is located at a sideline distance of y_{obs}. For the bulk of the results, $\theta = 45°$, but will range from 5° to 55° in an attempt to assess the average noise reduction with phase control. All propellers are rotating at a rate of 8,000 RPM yielding a blade passage frequency (BPF) of 400 Hz. The advance ratio is set to $J = 0.6$ (32 m/s forward flight speed), which is near maximum propeller efficiency.[5] Also, the propeller axes are aligned with the flight direction such that the propeller angle of attack is zero. Only the forward flight mode is considered. Modeling VTOL and transition to forward flight are part of ongoing work.

3. METHODS

Several steps are involved in generating the data, including data manipulation and two methods built across existing tools. Prior to implementation, a set of consistency checks are performed to verify each process. This section begins by explaining the source noise prediction, followed by details on the system noise prediction and auralization.

3.1 Source Noise Modeling and Auralization

The Propeller Analysis System of NASA's Aircraft NOise Prediction Program[6] (ANOPP-PAS) is used to obtain the individual steady blade pressure loadings at the given flight condition via blade element momentum theory (see Pascioni & Rizzi[5] for details). No vehicle installation effects are modeled, i.e., the inflow is a uniform freestream. Noise due to unsteady loading or other vehicle noise sources such as electric motor noise[7] are also not considered.

The surface pressure and blade geometry then serve as input into ANOPP2[8] to compute the acoustic pressure time history of a single propeller using Farassat's F1A formulation[9] of the Ffowcs Williams-Hawkings equation.[10] For each propeller, a set of observers at a fixed radius of $12R$ (R being the propeller blade radius) is defined with a 5° resolution. The set of observers and associated pressure data are referred to as a source hemisphere. The source time record at each observer location has 600 samples over a full rotation period (7.5 ms) resulting in a sample rate of 80 kHz. In the following, a discrete Fourier transform with a time window of one blade passage is applied to give the magnitude and phase of each harmonic. The harmonic series is truncated at the fifth harmonic as the amplitudes fall off rapidly with increasing harmonic. Figure 2 gives the polar directivity of these frequencies for a single propeller, peaking in the aft quadrant at $\phi \approx 105°$. As mentioned, the propeller angle of attack is zero; thus, directivity of each propeller is independent of θ.

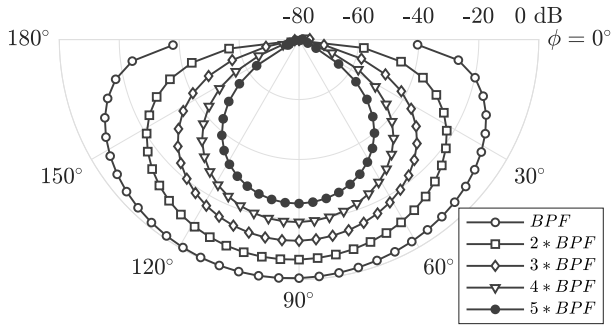

Fig. 2 – Polar directivity prediction of a single GL-10 propeller for the BPF and subsequent harmonics at 8,000 RPM, $J = 0.6$.

The results that follow use two methods, summarized in Fig. 3, to propagate the acoustic source hemispheres to the ground observer. Following the upper path of the flow chart, the vehicle noise is estimated by distributing $N_p = 10$ instances of the source hemisphere corresponding to the propeller layout, in which N_p is the number of propellers. The data are projected onto a "vehicle" hemisphere to superpose the pressure time histories.[5] This projection adjusts the pressure amplitude and imposes a time delay, individually for each propeller, based on straight ray propagation. The data are linearly interpolated on the surface of the

source hemispheres between data points. An additional time offset per propeller can be enacted to account for their desired azimuthal position offset, ψ. Sound pressure levels (dB) for each 1/3-octave band are computed on the vehicle hemisphere and read into the ACoustic Data Module (ACD) of ANOPP to prepare the data. The global hemisphere is subsequently propagated to the stationary observer using ANOPP-PRO to simulate a flyover event. Metrics are then computed within ANOPP-GROUND. This method is used in section 4.1.

The second method (lower portion of the flow chart) applies to section 4.2 and uses the NASA Auralization Framework (NAF).[11] The NAF is an open-architecture software that can simulate sounds from moving sources, accounting for spherical spreading loss, absolute time delay (giving rise to Doppler shift), atmospheric absorption, and ground plane reflection. Recently, the ANOPP2-NAF interface[11,12] has been built to couple auralization processes with noise predictions. The same basic auralization approach used by Krishnamurthy et al.[13] is employed here, with additional steps to set the azimuthal position offsets of the individual propellers and the transition between phase sets associated with different optimized regions. First, the pressure time history of a full propeller revolution is read from the ANOPP2 source hemisphere. A subsection of the pressure time history corresponding to a single blade passage, closest to the specified phase ψ, is selected. For each observer point on the hemisphere, the NAF periodic plugin performs a Fourier transform of the selected samples to obtain the magnitudes and phases of the harmonic sequence. These data are stored in an interpolation table. Next, the flight path is queried to find the time-dependent emission angle in order to calculate a time-dependent magnitude and phase from the interpolation table (NAFSynth). A spherical interpolation scheme[13] handles the phase wrapping appropriately. An additive synthesis method generates the acoustic pressure time history at the source for each propeller. Finally, the NAF Gain-Time Delay-Filter module (NAFGTF) delays and attenuates the signal by the propagation time and spreading loss, respectively. At the ground observer, propeller signatures are summed and certification-type metrics are computed using the ANOPP2 Acoustic Analysis library. Metrics computed using this library are equivalent to those obtained using ANOPP-GROUND.

Note that atmospheric absorption was not modeled in the following because its effect was found to be less than 1 dB at the propagation distances of interest. Similarly, atmospheric turbulence[14] was also investigated and found to have a negligible effect on the results. For observer locations above the ground, reflections are modeled as a simple hard boundary having infinite impedance.

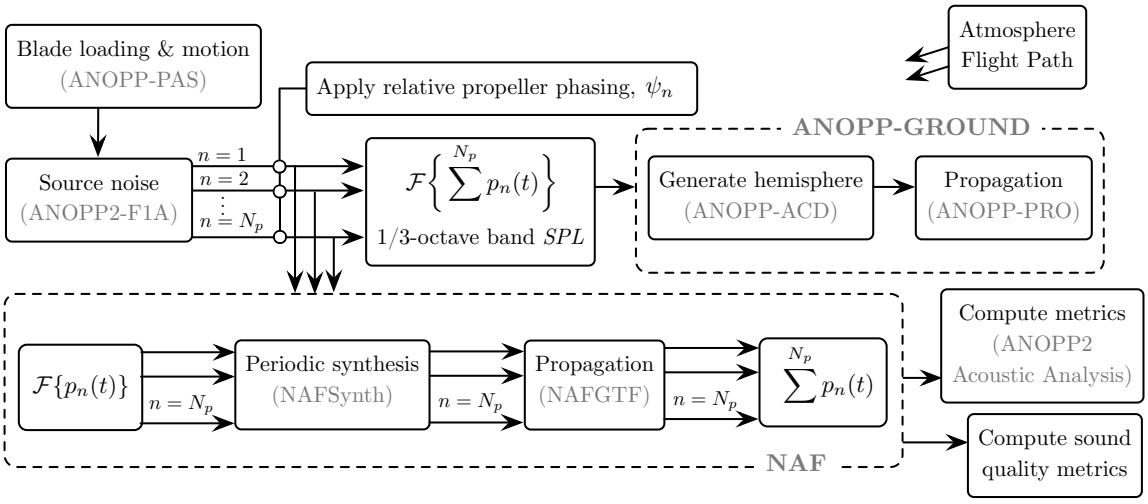

Fig. 3 – Flow chart of data generation and manipulation.

3.2 Propeller Phase Control

Controlling the relative azimuthal positions of propellers has shown promise for minimizing cabin noise for two and four propeller transports.[1–3,15] However, the authors are not aware of any analysis or system having an objective of reducing community noise. While this technology has not yet been employed, there may be significant noise benefits with little to no loss in performance (other than the additional complexity of the motor controllers). In addition, the large number of propellers typically found in DEP systems likely increases authority over directivity modification. However, the number of propellers of the GL-10 makes direct computation of all possible phase combinations intractable. To limit computational expense and following work of the antenna community (see, for example, Ares et al.[16] and Boeringer & Werner[17]), optimization techniques are used to solve for the phase angle sets that minimize community noise.

The optimization process employs the interior point algorithm[18] via the `multistart` method of `fmincon`[19] in Matlab. Additional details on this process are given in Pascioni & Rizzi.[5] The objective function is specified as the minimum average sound pressure level over a subset of ground observers. To test if phase control has enough authority to 'steer' acoustic energy away from a given direction, 45° wedges of emission angles are considered per optimization run. Figure 4 gives the noise contours of optimized phase sets for four wedges that cover the starboard side of the vehicle. Note that the optimization was not performed on flyover events; rather, the vehicle-to-observer position remain fixed and therefore the Doppler shift was not included. No attempt was made to enforce continuity of vehicle directivity across the optimization boundaries. The optimized phase sets for this flight condition are summarized in Table 1. The ground noise contour averaged over 5,000 random phase combinations is also given for reference. As shown, phasing can effectively reduce the tonal noise levels by approximately 20 dB averaged over a given wedge under these ideal conditions. In each case of Figs. 4(b-e), the action of optimizing a particular wedge is accompanied by an increase in the maximum SPL at some other nonoptimized location.

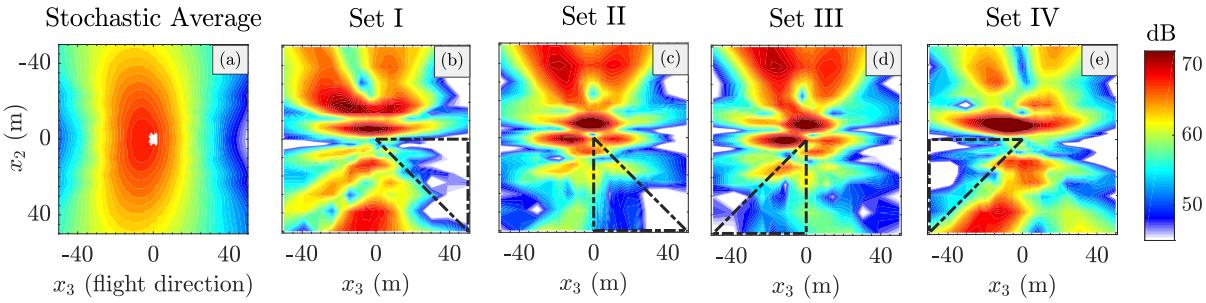

Fig. 4 – Sound pressure level, L, of the (a) stochastic average and (b-e) GL-10 under phase control illustrating directivity modification of the blade passage frequency on the ground plane at 8,000 RPM, J = 0.6. The relative phases are summarized in Table 1, and the outlined regions are the observers given to the optimization for noise minimization.

Table 1 – Azimuthal blade positions, ψ, relative to propeller n_1, defined about the full rotational azimuth; hence, $\max\{\psi\} = 120°$ as there are three blades per propeller. Each angle is defined in the direction of rotation.

		Propeller									
		n_1	n_2	n_3	n_4	n_5	n_6	n_7	n_8	n_9	n_{10}
ψ,	*Set I*	0.0°	53.8°	79.0°	102.7°	38.4°	22.1°	53.6°	4.8°	5.8°	62.4°
	Set II	0.0°	73.2°	114.8°	84.3°	23.9°	116.6°	27.9°	1.3°	28.5°	52.7°
	Set III	0.0°	87.9°	1.8°	96.9°	30.1°	118.4°	37.6°	112.0°	39.8°	64.8°
	Set IV	0.0°	59.1°	96.5°	41.2°	77.2°	16.9°	23.6°	99.3°	103.6°	37.0°

It is important to reiterate the assumptions that have been made thus far. As mentioned, realistic source characteristics driven by unsteady loading either due to installation effects or turbulence are neglected. These are expected to be important for this vehicle configuration, particularly for propellers with low tip Mach numbers. Also, constructive interference modeling assumes unit coherence between all propellers. Coherence is likely to drop with separation distance (or more accurately, separation distance multiplied by the acoustic wavenumber), particularly between the wing and tail propellers. Coherence can also be degraded due to the error in the motor RPM and/or phase controller. To this end, the 20 dB maximum reduction in noise levels as indicated by Fig. 4 is not expected in practice, but these ideal trends show this technology to be promising at this time.

4. RESULTS

The effect of random propeller phasing, a common characteristic amongst current vehicles, is first estimated via a flyover using a statistical representation of the vehicle propeller noise. This is done to prescribe a noise envelope of the operating state. Phase control is then imposed to demonstrate how existing tools can be used to study potential benefits. The auralized signals produced in the following sections can be downloaded from the internet.[20]

4.1 Effect of Random Propeller Phase

A Monte Carlo simulation is computed to understand the noise sensitivity to phase under the aforementioned assumptions. Data from 5,000 combinations of random phase are stored on the vehicle hemisphere as mentioned in section 3.1. The 5,000 cases are averaged on the hemisphere on a per-observer basis to represent the average sound pressure level expected as a function of emission angle. The noise prediction of a single flyover event, along the path described in Fig. 1(b) in which $\theta = 45°$, is made using this statistical source representation. Figure 5(a) gives the average A-weighted sound pressure level, L_A, as a function of reception time. The observer is on the ground, thus these results include a 6 dB increase due to pressure doubling.

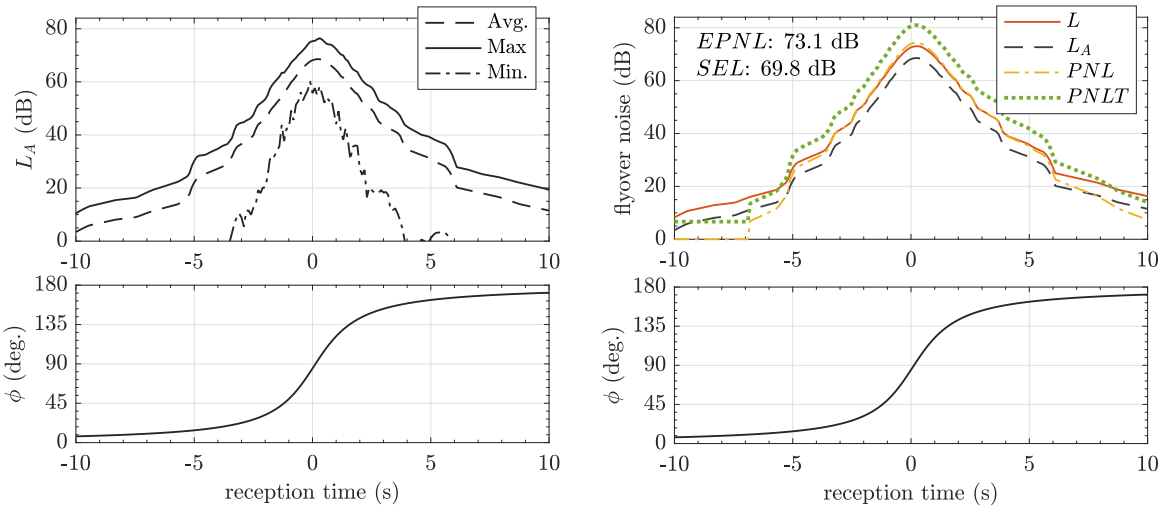

Fig. 5 – Flyover of the statistical representation of the GL-10 showing the (a) minimum, average, and maximum L_A per point along the flight path over 5,000 random phase combinations. Additional metrics are given in (b) for the average case. The observer azimuth is $\theta = 45°$ and the vehicle position is represented by the polar angle ϕ for each figure.

The peak L_A is 68.6 dB and occurs just after the vehicle's center of gravity becomes perpendicular to the observer ($\phi = 93°$). This is consistent with the aft location of the peak

directivity for a single propeller, with a slight shift upstream due to the propeller layout. Figure 5(a) also shows the minimum and maximum level produced by any given phase combination per point on the flight path using the same statistical source. These data should be thought of as envelope boundaries. The results in the following section employing phase control are expected to fall in the band outlined by the average and minimum cases.

A noise metric (or combination thereof) that best captures human annoyance has not yet been established for UAM-class vehicles. Given this, additional metrics computed from the 1/3-octave band spectra are plotted in Fig. 5(b) for the average case just described. A-weighting tends to reduce the levels fairly uniformly over the flight path. That is, the difference in L_A and the unweighted sound pressure level, L, is approximately 4.5 dB. Most of this difference is associated with the dominant BPF tone at 400 Hz, corresponding to an A-weighted correction of -4.8 dB. Note that the Doppler shift has little effect on A-weighting since the vehicle is traveling less than Mach 0.1, so it is not included. Perceived noise level (PNL) is very similar to L, while $PNLT$ is largest, peaking at 81.0 dB due to the tonal nature of the source noise. The tone penalty of 6 dB is nearly uniform across the duration of the flyover. Certification-type metrics accounting for duration are also computed, resulting in effective perceived noise level, $EPNL$, and sound exposure level, SEL, at 73.1 and 69.8 dB, respectively.

4.2 Sideline Flyover with Phase Control

Auralizations of GL-10 flyover noise are performed using the NAF for the optimized propeller phase sets in Table 1. Figure 6(a) compares the noise produced by each phase set. Even though these data give information only at one observer azimuth ($\theta = 45°$), the trends are as expected. For instance, just after the first phase transition ($\phi = 45°$, $t = -1.2$ s), set II performs the best relative to the other phase sets until the aircraft is perpendicular to the observer at $\phi = 90°$. After the second transition ($\phi = 90°$, $t = 0.13$ s), set III results in the lowest levels. Finally, after the last phase transition ($\phi = 135°$, $t = 1.5$ s), set IV outperforms sets I and II but not set III at this azimuthal angle. Recall that each set is optimized over a set of observer azimuth angles; hence, only in an average sense is set IV intended to be the lowest of the combinations for these aft emission angles (per Fig. 4).

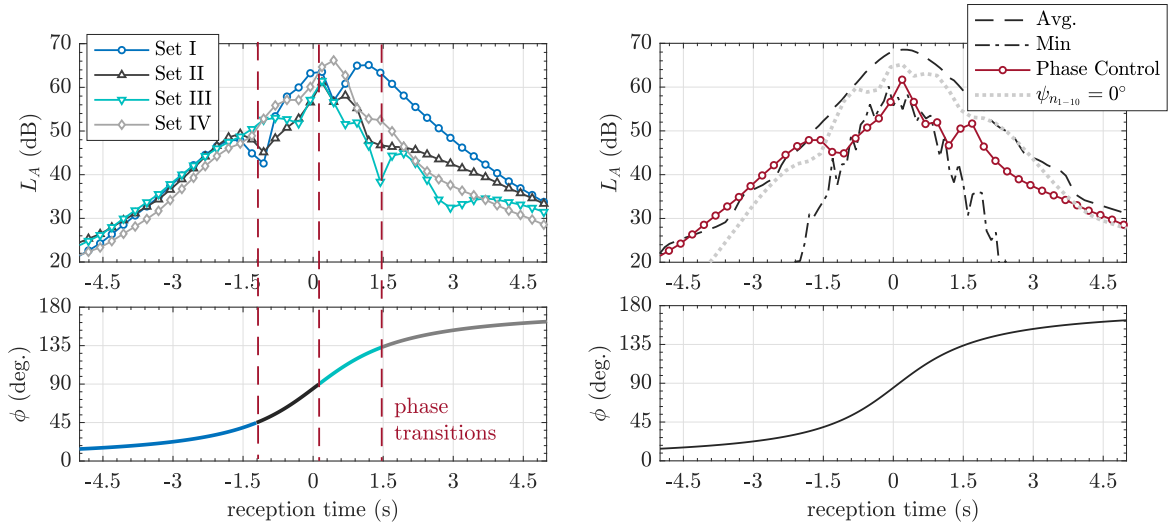

(a) (b)

Fig. 6 – Flyover at $\theta = 45°$ with (a) individual phase sets I-IV and (b) transitioning from each set along the flight path, compared to the statistical source representation of Fig. 5 and the fixed in-phase condition.

Figure 6(b) shows a flyover implementing phase control, i.e., switching through the optimal phase sets that correspond to a given polar emission angle. The transition duration is 0.2 s,

which is chosen to represent typical time responses of a motor phase controller. Clearly, the noise levels are significantly lower than the average over the emission angles used for optimization, corresponding to reception times between $t = -2.6$ and $t = 2.1$ s. Before and after these reception times, the levels are dominated by spherical spreading. Comparing these metrics to the average case, greater than 10 dB reduction is indicated. The case in which the relative propeller phases are equal ($\psi_{n_{1-10}} = 0°$) is also given in Fig. 6(b) as an additional reference point, since fixing the relative phase throughout the flight path is likely easier to implement. While reductions in noise levels are not as good as with phase control, fixing the phase looks to yield similar results to the average phase case. Note that this simple comparison does not necessarily hold for different vehicles, or more specifically, different blade passage frequencies and/or propeller spacing.

Additional insight into the characteristics and behavior of the noise, particularly at the phase transitions, can be obtained by looking at the spectrogram and pressure time history. Moving the observer to 1.2 m above the ground allows investigation of the effect of ground reflections. The spectrogram shown in Fig. 7(a) indicates the five harmonics included in the source synthesis, the roll-off in amplitude with increasing harmonic (refer to Fig. 2), and the Doppler shift associated with the movement of the vehicle. The interference pattern produced by the ground plane reflection is not pronounced due to the lack of a broadband noise component.

More interesting is the pressure time history envelope at the observer, Fig. 7(b). A flyover of more conventional aircraft would more or less see a steady rise and fall governed by spreading loss and source directivity as the vehicle passes the observer. The envelope shown here, however, has an unsteady character due to the spatially complex interference pattern (see Fig. 4). There is a noticeable jump in sound pressure and loudness (not shown) at the transition between phase sets III and IV. Such a jump could have a startling effect on an observer. The optimization scheme used in this effort is performed independently for each zone. If such jumps are later found to contribute to annoyance, an alternative optimization scheme that takes into account the transition between zones would be appropriate.

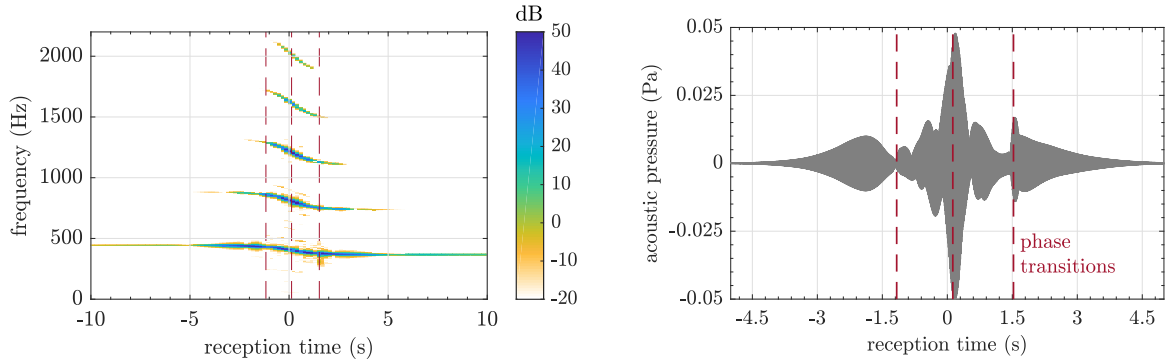

Fig. 7 – Flyover of the GL-10 under phase control at $\theta = 45°$; (a) spectrogram and (b) envelope of pressure time history at an observer 1.2 m above the ground. Ground reflections from a hard surface are included.

Finally, flyovers at several additional sideline observer offsets ($\theta = 5°$ to $55°$) are simulated to provide insight into overall trends of phase control. Figure 8(a) shows that the energy is spread more evenly across reception times as θ is increased. This is because ϕ changes more gradually, a result of the source-to-observer geometry. For the same reason, levels are highest at low θ. Fig. 8(b) provides an alternative means of comparing potential benefits of optimized phase control. Shown here are SEL and $EPNL$ differences of each flight path relative to the statistical averaged source along that same path. Some reduction is found at all azimuths, with greatest reductions being achieved at $\theta = 45°$ and $55°$. Note that the $5°$ case is very close

to both the edge of the optimization boundary and being directly below the aircraft. While phase control does not perform well here, the optimization region could be changed if this is deemed the most important region to control.

It is worthwhile to note here that the reduction in sound pressure level at the ground observer is not accompanied by a reduction in performance, as all propellers rotate at a constant rate except over the short transitions. Consequently, the power consumed is neither increased or decreased, and the velocity and time to destination are unaffected.

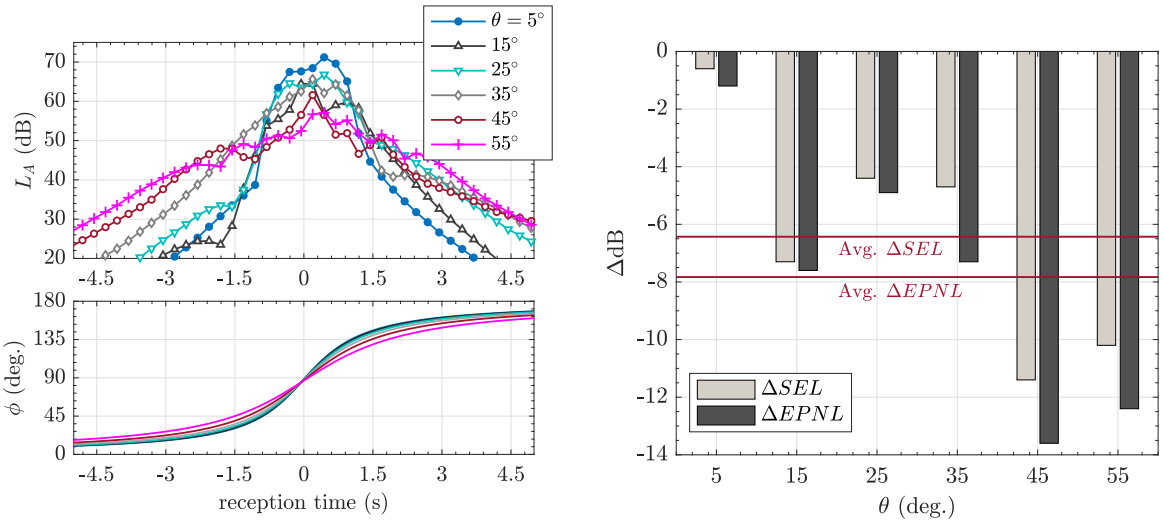

(a) (b)

Fig. 8 – Flyover of the GL-10 under phase control at (a) various sideline positions; (b) comparison of certification-type metrics using the stochastic average of Fig. 5 as the reference.

5. CONCLUSIONS

A method to auralize the tonal noise of a distributed propulsion UAM-like vehicle under phase control is presented. Using ANOPP-PAS and ANOPP2, the source noise is first derived using Farassat's F1A solution from the blade pressures computed via blade element momentum theory. The NAF is used to synthesize the source noise of a continuously varying pressure time history, and propagate that to an observer on or near the ground. From the phase-optimized azimuthal blade settings, flyovers are simulated giving the ability to transition from different phase sets which correspond to low-noise solutions over specific observer wedges. As the source noise prediction continues to mature, the methods described here will allow users to study distributed propulsion UAS or UAM vehicles using certification-type metrics, sound quality metrics, or tests for human acceptance. Also as important, the suitability of phase control as a noise reduction technology could be studied for any vehicle of interest, as some configurations may be better suited to reap the benefits. Under the current source noise assumptions, the GL-10 can obtain an average reduction of 6.4 dB in SEL and 7.8 dB in $EPNL$ of a flyover under the operating conditions chosen for this work.

During this study, several additional paths for improvement have surfaced. First, a more in-depth analysis of the transitions would prove useful to understand whether the transients in the source characteristics are significant enough to affect human perception of the sound. Second, the optimization process could be built upon different metrics, e.g., L_A, SEL, or others which correlate with human response, including audibility in the presence of ambient noise. Third, the width of the observer wedge used for optimization should be understood. Assuming a motor controller without limitations, a smaller wedge may prove more beneficial, as well as overlapping subsets so as to avoid transitions accompanied by high noise levels.

ACKNOWLEDGMENTS

This work was supported by the NASA Aeronautics Research Mission Directorate, Revolutionary Vertical Lift Technology Project. The authors would like to thank Dr. Len Lopes from NASA Langley Research Center for his assistance with ANOPP2.

REFERENCES

1. J. Johnston, R. Donham, and W. Guinn. Propeller signatures and their use. *Journal of Aircraft*, 18:934–942, 1981.

2. B Magliozzi. Synchrophasing for cabin noise reduction of propeller-driven airplanes. In *8th AIAA Aeroacoustics Conference*, 1983.

3. C. Fuller. Analytical model for investigation of interior noise characteristics in aircraft with multiple propellers including synchrophasing. *Journal of Sound and Vibration*, 109 (1):141–156, 1986.

4. W. Fredericks, M. Moore, and R. Busan. Benefits of hybrid-electric propulsion to achieve 4X increase in cruise efficiency for a VTOL aircraft. In *AIAA Aviation Technology, Integration, and Operations (ATIO) Conference*, AIAA Paper 2013-4324, 2013.

5. K. Pascioni and S. Rizzi. Tonal noise prediction of an unmanned aerial vehicle. In *24th AIAA/CEAS Aeroacoustics Conference*, 2018, *submitted*.

6. W. Zorumski. Aircraft noise prediction program theoretical manual, part 1. NASA TM-93199, 1982.

7. D. Huff, B. Henderson, and E. Envia. Motor noise for electric powered aircraft. In *22nd AIAA/CEAS Aeroacoustics Conference*, AIAA Paper 2016-2882, 2016.

8. L. Lopes and C. Burley. ANOPP2 users manual. NASA TM-2016-219342, 2016.

9. F. Farassat. Theory of noise generation from moving bodies with an application to helicopter rotors. NASA TR-R-451, 1975.

10. J. Ffowcs Williams and D. Hawkings. Sound generation by turbulence and surfaces in arbitrary motion. *Phil. Trans. R. Soc. Lond. A*, 264(1151):321–342, 1969.

11. A. Aumann, B. Tuttle, W. Chapin, and S. Rizzi. The NASA auralization framework and plugin architecture. In *Internoise 2015*, 2015.

12. B. Tuttle, A. Aumann, S. Rizzi, J. Jones, and L. Lopes. Flyover noise simulation using nasa's coupled aircraft system noise prediction and auralization frameworks. In *INTER-NOISE and NOISE-CON Congress and Conference Proceedings*, volume 255, pages 414–421. Institute of Noise Control Engineering, 2017.

13. S. Krishnamurthy, S. Rizzi, D. Boyd, and A. Aumann. Auralization of rotorcraft periodic flyover noise from design predictions. In *AHS International Forum 74*, 2018.

14. F. Rietdijk. *Auralisation of airplanes considering sound propagation in a turbulent atmosphere*. Ph.D. Dissertation, Chalmers University of Technology, 2017.

15. X. Huang, Y. Wang, and L. Sheng. Synchrophasing control in a multi-propeller driven aircraft. *Journal of Engineering for Gas Turbines and Power*, 136(11), 2014.

16. F. Ares-Pena, J. Rodriguez-Gonzalez, E. Villanueva-Lopez, and S. Rengarajan. Genetic algorithms in the design and optimization of antenna array patterns. *IEEE Transactions on Antennas and Propagation*, 47(3):506–510, 1999.

17. D. Boeringer and D. Werner. Particle swarm optimization versus genetic algorithms for phased array synthesis. *IEEE Transactions on antennas and propagation*, 52(3):771–779, 2004.

18. R. Byrd, J.C. Gilbert, and J. Nocedal. A trust region method based on interior point techniques for nonlinear programming. *Mathematical Programming*, 89(1):149–185, 2000.

19. *MATLAB Optimization Toolbox, version 9.3.0.713579 (R2017b)*. The Mathworks, Inc., Natick, Massachusetts, 2017.

20. Aircraft flyover simulation. http://stabserv.larc.nasa.gov/flyover/. NASA, 2018.